Measurements of Laser-Speckle–Induced Perturbations in Laser-Driven Foils

S. G. Glendinning *M. H. Key*[*] *B. A. Remington*

S. N. Dixit *J. D. Kilkenny* *R. J. Wallace*

B. A. Hammel *J. P. Knauer*[**] *S. V. Weber*

D. H. Kalantar *D. M. Pennington*

Introduction

Growth of modulations in an inertial confinement fusion (ICF) capsule, whether initially due to capsule surface finish or drive nonuniformity, may fatally disrupt an ICF implosion by causing cold shell material to mix into the fuel.[1,2] When a capsule is driven by x rays produced inside a hohlraum, the dominant modulations are seeded by the capsule surface finish. When laser light directly drives the capsule, the modulations in the driver may be significant. Recent experiments[3,4] have reported reductions in imprint using smoothed laser beams, i.e., laser beams that have a reduced level of spatial nonuniformities. Another technique for reducing imprint has been the use of foams and gold layers.[5,6] In this article, we report measurements that quantified the equivalence between laser-imprinted modulations and surface perturbation.

Experimental Description

In our experiment, we used laser ablation to accelerate 20-μm-thick CH_2 foils with one arm of the Nova laser at 0.53-μm wavelength. This arm was smoothed with a random phase plate (RPP)[7] and spectral dispersion[8] (SSD), for three different bandwidths in separate experiments: 0.003 THz (the intrinsic bandwidth, introduced by the pulse-shaping system), 0.6 THz, and 0.9 THz. A diffraction grating gave 0.086-μrad/THz dispersion and a temporal skew of 110 ps to the pulse front (that is, one side arrived earlier than the other). The beam was split into nine segments, each independently steered in space with a glass wedge to form a flat-topped intensity distribution. We measured the time-integrated laser modulation level from an equivalent target-plane image of the beam. The drive pulse was a linear 1-ns ramp to about 10^{14} W/cm^2, held constant at this level for 2 ns.

The shock reached the back surface of the 20-μm-thick foil at about 0.7 ns after the start of the laser pulse. The foil then accelerated at about 50 μm/ns^2, allowing for 2 ns of constant acceleration to study Rayleigh–Taylor (RT) growth. We measured the areal-density modulations on the foils by conventional x-ray backlighting. We used a gated pinhole camera with 8-μm and 100-ps resolution,[9] which provided up to 12 frames per shot with arbitrary time spacing. The x-ray backlighter[10] was a uranium disk illuminated by a second 0.53-μm-wavelength Nova beam (smoothed with an RPP) at about 10^{15} W/cm^2, giving a broad spectrum peaked at ~1 keV.

Simulations

To examine the predicted evolution of imprinted modes compared to surface modes, we used the two-dimensional code LASNEX[11] to separately predict the evolution of a surface single mode and of an imprinted single mode (produced by modulating the incident laser intensity) under the same drive conditions. The LASNEX results showed that the evolution of a laser-imprinted single mode parallels that of a surface single mode after the shock reaches the back surface t_s (see Fig. 1). This suggested that, for our conditions, the laser imprint could be calibrated to an equivalent surface finish. We also used the simulations to estimate the correspondence of a spatial amplitude η with a measured modulation in optical depth $\Delta\tau$, finding that $\eta/\Delta\tau = 10\ \mu\text{m}/\tau$ after t_s. This allowed us to make use of the Haan criterion[12] to establish the onset of multimode nonlinear saturation. We restricted our analysis to data that were estimated to be in the linear regime.

[*] Rutherford Appleton Laboratory and University of Oxford, United Kingdom.
[**] Laboratory for Laser Energetics, Rochester, New York.

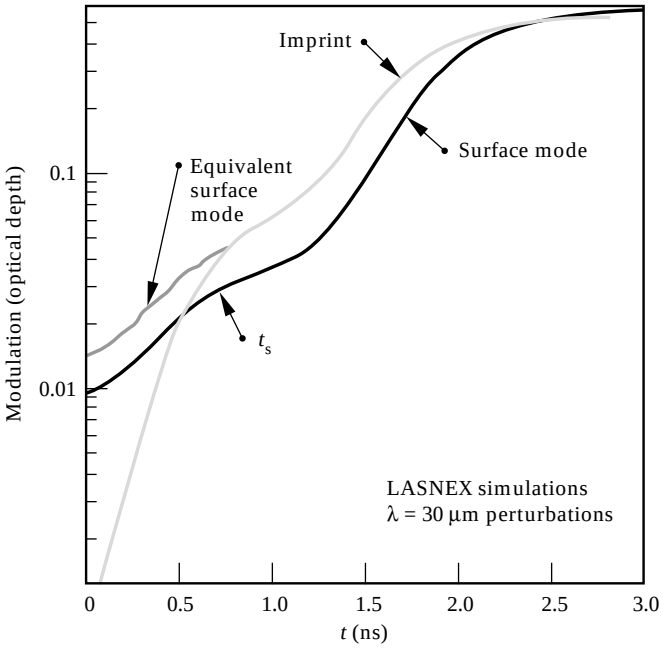

FIGURE 1. LASNEX simulation of optical-depth modulation vs time for a single surface mode and a single imprinted mode of the same wavelength (30 μm). The growth rate between t_s (0.7 ns) and the onset of saturation at $\Delta\tau = 0.3$ is 2.2 ns^{-1} for the imprinted mode and 2.5 ns^{-1} for the surface mode. While the imprint begins at zero modulation, an equivalent surface mode would begin at 0.02. (20-03-0796-1564pb01)

We analyzed each frame by converting the film density to exposure; removing the long-scale-length backlighter shape; filtering out noise with a parametric Wiener filter; converting to the natural logarithm of exposure; and taking the two-dimensional power spectrum of the result. A typical image of ln(exposure) is shown in Fig. 2(a). A vertical profile, which is the horizontal average of the image, is shown in Fig. 2(b). The surface mode in this case was $\lambda = 30$ μm (mode 10, initial amplitude $\eta_0 = 0.25$ μm) with the modulation vector **k** vertical in the image, and the bandwidth was 0.9 THz. We removed the contribution of the surface mode by using a notch filter at the point in Fourier space where the surface mode appears. The same image with the surface mode removed is shown in Fig. 2(c) and its corresponding horizontal average is the dark gray line in Fig. 2(b). Figures 3(a) and 3(b) show the radial power spectra (azimuthal integrals of the two-dimensional power spectra) for this shot at three different times, the noise power spectrum (measured on a separate shot with an undriven foil), and the instrument modulation transfer function (MTF). The laser imprint was almost indistinguishable from the noise for the higher bandwidths at t_s (not shown), but subsequent growth gave clearly measurable modulations at later times. Figures 4(a) and 4(b) show the time-integrated power spectra of the laser speckle and the imprinted spectra at $t = 1.5$ ns as measured for the different bandwidths. As is characteristic with SSD, while there was smoothing at all modes, the higher modes were smoothed preferentially.

To test the LASNEX prediction that the evolution of a laser-imprinted mode parallels the surface mode after t_s, we examined the growth for several shots. Figure 5 shows the results for the shot of Figs. 2 and 3. The modulation amplitudes for the surface mode ($\lambda = 30$ μm), for the imprinted spectrum at mode 10, and for the root-mean-square (rms) of the ln(exposure) are shown as a function of time after the start of the laser pulse. We subtracted in quadrature the noise component due to the instrument and backlighter from the values for the imprint modes. The

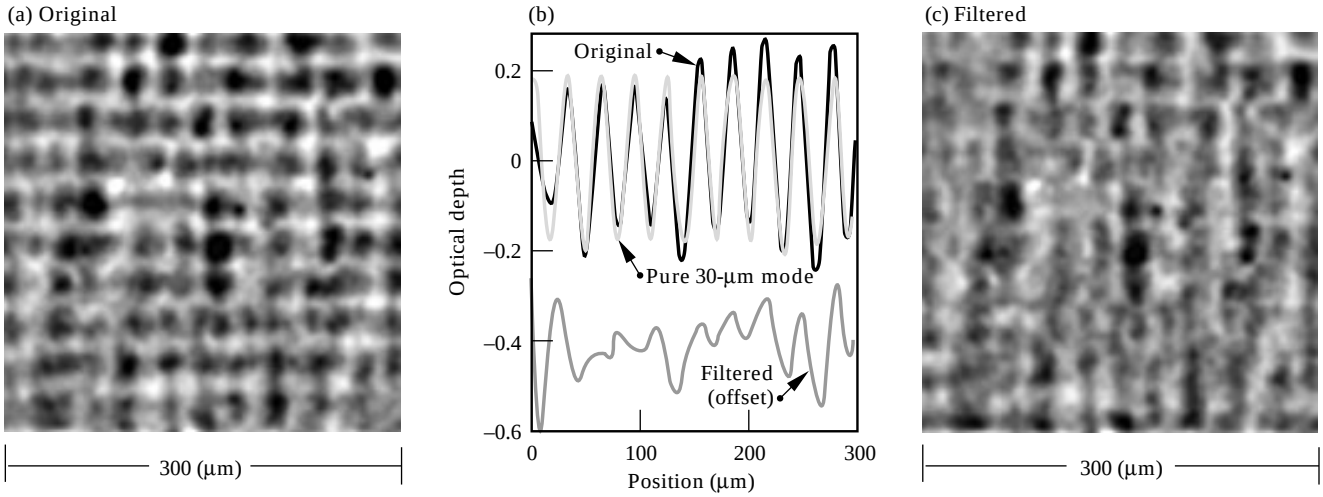

FIGURE 2. A single image from a framing camera radiograph at $t = 1.9$ ns (1.2 ns after t_s), shown in ln(exposure). (a) is the original image, with a $\lambda = 30$ μm, $\eta_0 = 0.25$ μm surface mode. The vertical profiles in (b) are made by horizontally averaging the images. In (b), the black curve is from (a) and the light gray curve is a pure 30-μm mode with $\Delta\tau = 0.2$ (optical depth), while the dark gray curve corresponds to (c). (c) has been digitally filtered to remove the $\lambda = 30$ μm mode in the vertical direction only. (20-03-0796-1565pb01)

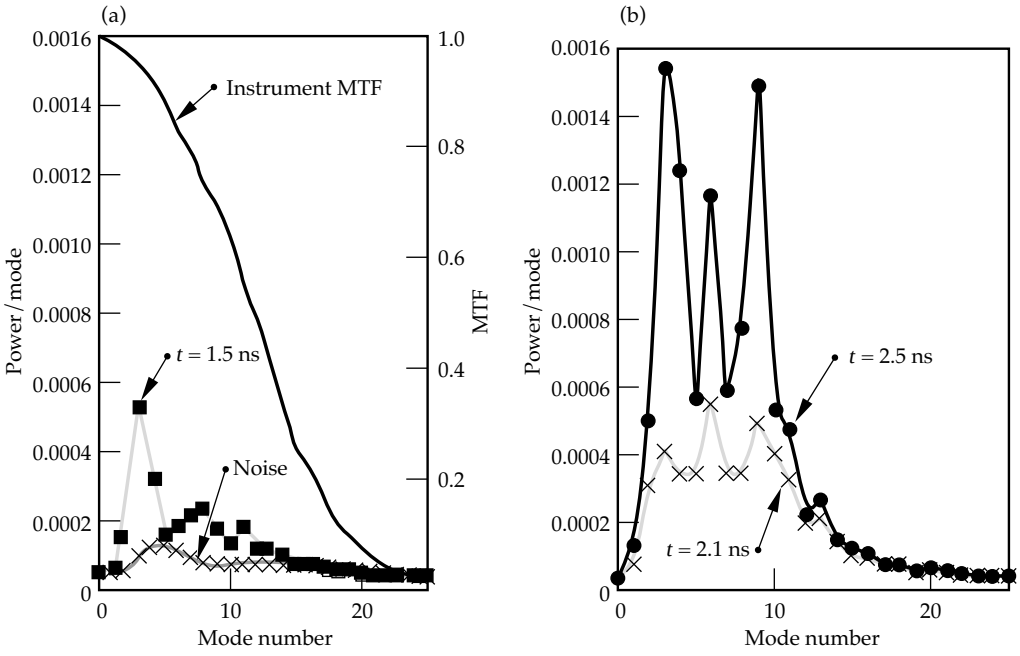

FIGURE 3. Azimuthally integrated radial profiles at three different times of the two-dimensional Fourier power spectra for the shot shown in Fig. 2. Also shown are the instrument noise (measured on a shot with an undriven foil) and the modulation transfer function (MTF) of the measurement system. The MTF uses the right axis. (20-03-0796-1566pb01)

two $\lambda = 30\ \mu$m modes from surface and imprint modulations grew at the same rate ($0.9 \pm 0.2\ \text{ns}^{-1}$). The rms grew at nearly the same rate ($0.8 \pm 0.2\ \text{ns}^{-1}$), suggesting that the growth rates for the dominant modes were similar.

At a given time in the linear regime, the ratio of the rms to the surface mode times the initial surface-mode amplitude gave the equivalent surface finish in microns at $t = 0$. The inferred rms surface finish was insensitive to the calibration wavelength we used, suggesting little variation in growth rate for the dominant wavelengths. We calculated the equivalent surface finish to be $0.26 \pm 0.07\ \mu$m with 0.9 THz of bandwidth on the drive laser, $0.51 \pm 0.24\ \mu$m with 0.6 THz bandwidth, and $1.24 \pm 0.27\ \mu$m with minimum bandwidth. Figure 6 shows these results vs bandwidth, along with the time-integrated rms modulation in the laser speckle. The imprinted-modulation rms appeared to decrease only about half as fast as the laser modulation as a function of bandwidth.

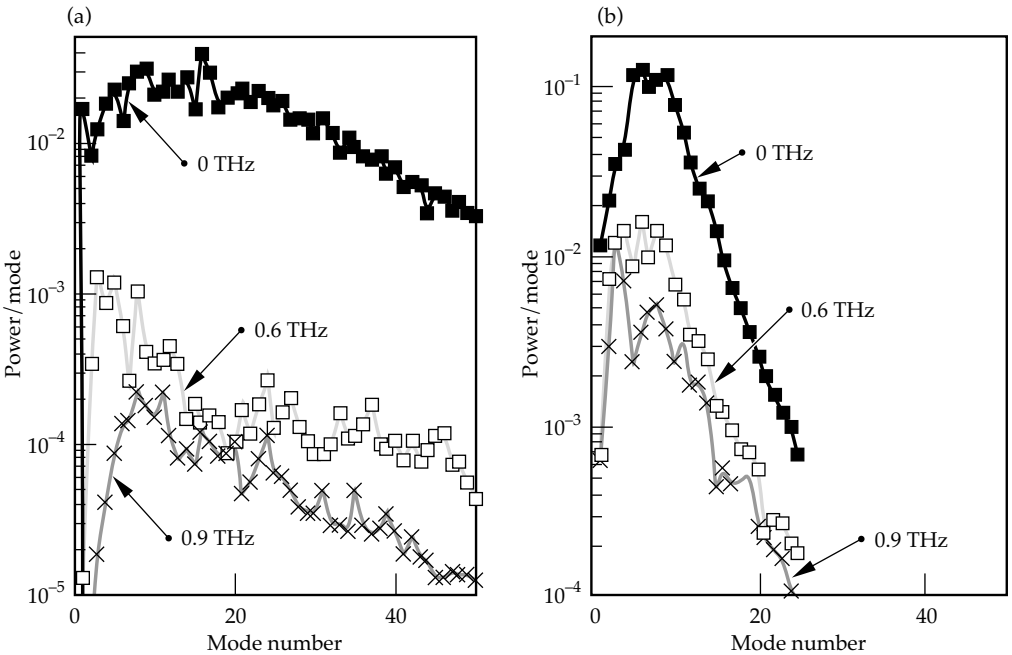

FIGURE 4. Power spectra of (a) the laser spots and (b) the imprinted modulation, converted to initial surface amplitudes, for the three bandwidths. (20-03-0796-1567pb01)

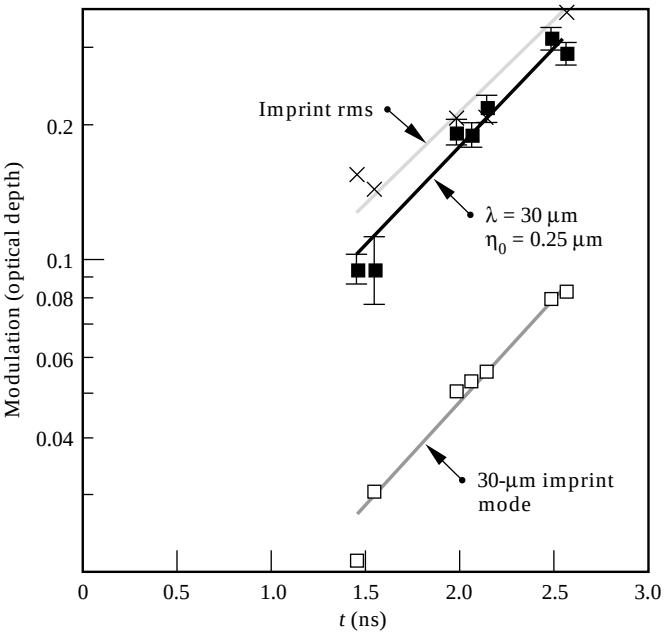

FIGURE 5. Modulation amplitudes for the shot shown in Figs. 2 and 3 vs *t*. The surface mode (shown with characteristic error bars), the imprinted mode at the same wavelength, and the rms grow at the same rate. (20-03-0796-1568pb01)

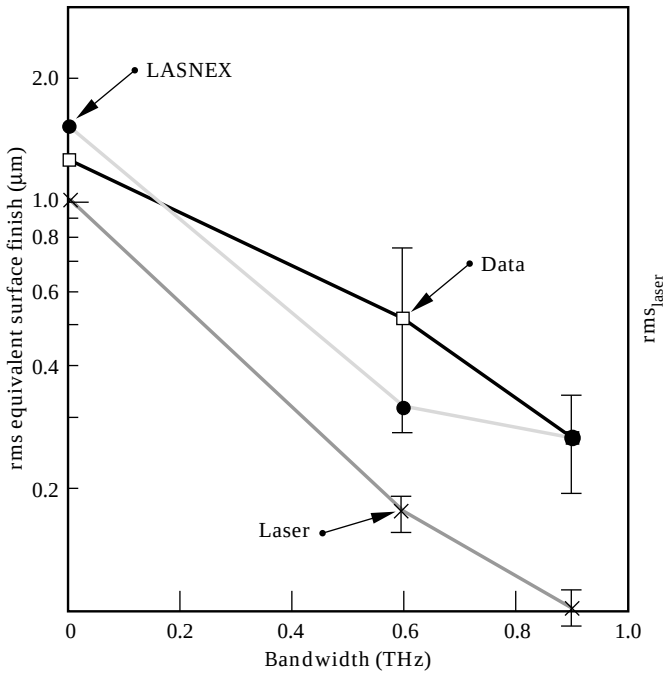

FIGURE 6. Equivalent surface finish for three bandwidths, as measured and simulated. The measured time-integrated laser-rms modulation vs bandwidth is also shown. The lines are a guide to the eye. (20-03-0796-1569pb01)

We used LASNEX to simulate the equivalent surface finish due to the laser imprinted modulations. The single-surface-mode simulation was done separately from the laser-imprint simulation. Since LASNEX is a two-dimensional code, the laser speckle is represented by a one-dimensional slice of the predicted laser-modulation pattern. With minimum bandwidth, the speckle is isotropic and the direction of the slice is not important. When SSD was added to the simulation, we used two directions—parallel and perpendicular to the direction of dispersion—and averaged the resulting predictions. The simulations propagated the measured backlighter spectrum through the simulated package and convolved the result with the instrument response function. The results are also shown on Fig. 6.

Conclusions

The predictions agreed with the experimental results. In particular, the predicted imprinted modulations did not decrease as rapidly with bandwidth as the time-integrated laser modulation. This effect has also been observed in experiments using a different measurement technique.[13,14] One possible explanation is the thermal smoothing of the drive modulations in the region between the laser light deposition and the ablation surface. In this region, the energy is propagated by electron thermal conduction and nonuniformities are smoothed inversely with the spatial scale of the nonuniformity. Thus, the minimum-bandwidth case showed more thermal smoothing because more of the laser modulation is at smaller spatial scales. If we calculate the laser time-integrated smoothing level including only lower modes (spatial structure > 30 μm), the rate of decrease of target imprint and the laser time-integrated smoothing level with increased bandwidth is the same. This suggests that the thermal smoothing for this experiment is most effective for modes with $\lambda < \sim 30\ \mu$m. Unfortunately, the instrument response greatly affects our ability to measure spatial structures less than 30 μm. While the LASNEX simulations predict that such structures are not present in the imprinted modulations, we cannot confirm this with the available data.

Summary

In summary, we have observed modulations due to laser speckle and we have shown that for a modest (less than a factor of three) amount of Rayleigh–Taylor growth, the speckle-imprinted modes grow at the same rate as a pre-imposed single-mode surface perturbation. We used this relationship to characterize the observed imprinted-rms modulation in optical depth as an equivalent surface finish for different bandwidths. The imprinted-foil modulations decreased with increasing bandwidth but not as rapidly as the time-integrated laser modulations, which is in agreement with numerical simulations. We suggest that this decrease is due to the additional smoothing of high spatial frequencies between the laser deposition region and the ablation surface.

Notes and References

1. J. Nuckolls, L. Wood, A. Thiessen, and G. Zimmerman, *Nature* **239**(5368), pp. 139–142 (1972).
2. M. M. Marinak, R. E. Tipton, O. L. Landen, T. J. Murphy et al., *Phys. Plasmas* **3** (5), pp. 2070–2075, (1996).
3. D. K. Bradley, J. A. Dellettrez, and C. P. Verdon, *Phys. Rev. Lett*. **68** (18), pp. 2774–1777 (1992).
4. J. D. Kilkenny, S. G. Glendinning, S. W. Haan, B. A. Hammel et al., *Phys. Plasmas* **1** (5), pp. 1379–1389 (1994).
5. M. Desselberger, T. Afshar-rad, F. Khattak, S. Viana et al., *Phys. Rev. Lett*. **68** (10), pp. 1539–1542 (1992).
6. R. J. Taylor, J. P. Dahlburg, A. Iwase, J. H. Gardner et al., *Phys. Rev. Lett*. **76** (10), pp. 1643–1646 (1996).
7. S. N. Dixit, I. M. Thomas, B. W. Woods, A. J. Morgan et al., *Appl. Optics* **32** (14), pp. 2543–2554 (1993).
8. S. Skupsky, R. W. Short, T. Kessler, R. S. Craxton, S. Letzring, and J. M. Soures, *J. Appl. Phys.* **66** (8), pp. 3456–3462 (1989).
9. O. L. Landen, P. M. Bell, J. A. Oertel, J. J. Satariano, and D. K. Bradley, *Ultrahigh- and High-Speed Photography, Videography, and Photonics '93* (SPIE—The International Society for Optical Engineering, Bellingham, WA, 1993; *Proc. SPIE* **2002)**, pp. 2–13.
10. S. G. Glendinning, P. Amendt, K. S. Budil, B. A. Hammel et al., *Applications of Laser Plasma Radiation II* (SPIE—The International Society for Optical Engineering, Bellingham, WA, 1995; *Proc. SPIE* **2523)**, pp. 29–39.
11. G. B. Zimmerman and W. L. Kruer, *Comments Plasma Phys. Controlled Fusion* **2** (2), pp. 51–61 (1975).
12. S. W. Haan, *Phys. Rev. A* **39** (11), pp. 5812–5825 (1989).
13. D. H. Kalantar, M. H. Key, L. B. Da Silva, S. G. Glendinning et al., *Phys. Rev. Lett*. **76** (19), pp. 3574–3577 (1996).
14. M. H. Key, *XUV Lasers and Applications* (SPIE—The International Society for Optical Engineering, Bellingham, WA, 1995; *Proc. SPIE* **2520)**, pp. 279–86.